Decoupled Deblurring Filter and its Application to Elastic Migration and Inversion

Zongcai Feng and Gerard T. Schuster, King Abdullah University of Science and Technology*
Wei Dai, Schlumberger

SUMMARY

We present a decoupled deblurring filter that approximates the multiparameter Hessian inverse by using local filters to approximate its submatrices for the same and different parameter classes. Numerical tests show that the filter not only reduces the footprint noise, balances the amplitudes and increases the resolution of the elastic migration images, but also mitigates the crosstalk artifacts. When used as a preconditioner, it accelerates the convergence rate for elastic inversion.

INTRODUCTION

Conventional migration can be considered as the first iteration of iterative least-squares inversion (Claerbout, 1992). The migration operation does not compute the Hessian inverse so the image suffers from amplitude distortion, strong footprint noise and blurring effects (Nemeth et al., 1999; Aoki and Schuster, 2009). In addition, the multiparameter migration image suffers from crosstalk artifacts (Operto et al., 2013).

The Hessian inverse are usually too expensive to compute and store for large-scale 3D applications. The simplest way to reduce the cost is to approximate it by a diagonal or diagonal-dominant matrix (Nemeth et al., 1999; Plessix and Mulder, 2004; Valenciano et al., 2006). Hu and Schuster (1998), Hu et al. (2001) and Yu et al. (2006) estimated the Hessian inverse by a series of local Hessian inverses in the wavenumber domain by assuming a locally layered medium. Guitton (2004) approximated the Hessian inverse with a bank of nonstationary matching filters. Similarly, Aoki and Schuster (2009) proposed a bank of localized stationary filters, called deblurring filters, to approximate the Hessian inverse. The deblurring filter is used to accelerate the convergence speed of least-squares migration (Aoki and Schuster, 2009; Dai et al., 2011).

We now develop a decoupled deblurring filter to estimate the multiparameter Hessian inverse. The filter estimates the near-diagonal elements of the submatrices of the Hessian inverse for the different parameter classes. Our decoupled deblurring filter is used to improve the elastic migration image quality and speed up the convergence of elastic linearized inversion (Duan et al., 2016; Feng and Schuster, 2017; Ren et al., 2017). The results show that the filter not only balances the amplitude, increases the resolution, but also reduces the crosstalk artifacts in the elastic migration images. It can also be used as a preconditioner to accelerate the convergence of elastic inversion.

THEORY

Multiparameter Hessian

The general theory for linearized seismic inverse theory and deblurring filter can be found in Aoki and Schuster (2009) and Dai et al. (2011). For two parameter classes, the forward modeling operator $\mathbf{L}$, reflectivity model $\mathbf{m}$ and corresponding migration image $\mathbf{m}^{\text{mig}}$ can be expressed as

$$\mathbf{L}=(\mathbf{L}_1,\mathbf{L}_2),\ \mathbf{m}=\begin{pmatrix}\mathbf{m}_1\\ \mathbf{m}_2\end{pmatrix},\ \text{and}\ \mathbf{m}^{\text{mig}}=\begin{pmatrix}\mathbf{m}_1^{\text{mig}}\\ \mathbf{m}_2^{\text{mig}}\end{pmatrix}. \tag{1}$$

The corresponding multiparameter Hessian $\mathbf{L}^T\mathbf{L}$ has the form

$$\mathbf{L}^T\mathbf{L}=\begin{pmatrix}\mathbf{L}_1^T\mathbf{L}_1 & \mathbf{L}_1^T\mathbf{L}_2\\ \mathbf{L}_2^T\mathbf{L}_1 & \mathbf{L}_2^T\mathbf{L}_2\end{pmatrix}. \tag{2}$$

The multiparameter migration image can be expressed as

$$\begin{pmatrix}\mathbf{m}_1^{\text{mig}}\\ \mathbf{m}_2^{\text{mig}}\end{pmatrix}=\begin{pmatrix}\mathbf{L}_1^T\mathbf{L}_1\mathbf{m}_1\\ \mathbf{L}_2^T\mathbf{L}_2\mathbf{m}_2\end{pmatrix}+\begin{pmatrix}\mathbf{L}_1^T\mathbf{L}_2\mathbf{m}_2\\ \mathbf{L}_2^T\mathbf{L}_1\mathbf{m}_1\end{pmatrix}. \tag{3}$$

Here, the first term on the right-hand side represents a blurred version of the actual reflectivity model, while the second term accounts for the crosstalk artifacts by parameter coupling.

Decoupled deblurring filter algorithm

The multiparameter Hessian inverse $(\mathbf{L}^T\mathbf{L})^{-1}$ can be written as a combination of four submatrices

$$(\mathbf{L}^T\mathbf{L})^{-1}=\mathbf{F}=\begin{pmatrix}\mathbf{F}_{1,1} & \mathbf{F}_{1,2}\\ \mathbf{F}_{2,1} & \mathbf{F}_{2,2}\end{pmatrix}, \tag{4}$$

where the submatrices $\mathbf{F}_{l,k}$ $(k,l=1,2)$ have the same dimension. Thus we have

$$\begin{cases}\mathbf{F}_{1,1}\mathbf{m}_1^{\text{mig}}+\mathbf{F}_{1,2}\mathbf{m}_2^{\text{mig}}=\mathbf{m}_1\\ \mathbf{F}_{2,1}\mathbf{m}_1^{\text{mig}}+\mathbf{F}_{2,2}\mathbf{m}_2^{\text{mig}}=\mathbf{m}_2\end{cases}. \tag{5}$$

For the decoupled deblurring filter, we seek four stationary local filters $\mathbf{f}_{k,l}$ to approximate the submatrices $\mathbf{F}_{l,k}$ in a window

$$\begin{cases}\mathbf{f}_{1,1}*[\mathbf{m}_1^{\text{mig}}]+\mathbf{f}_{1,2}*[\mathbf{m}_2^{\text{mig}}]=[\mathbf{m}_1]\\ \mathbf{f}_{2,1}*[\mathbf{m}_1^{\text{mig}}]+\mathbf{f}_{2,2}*[\mathbf{m}_2^{\text{mig}}]=[\mathbf{m}_2]\end{cases}, \tag{6}$$

where $[\ ]$ denotes the model or migration image in a window. The filter $\mathbf{f}_{l,k}$ is computed by constraining them to satisfy

$$\begin{cases}\mathbf{f}_{1,1}*[\mathbf{m}_1^{\text{mig\_ref}}]+\mathbf{f}_{1,2}*[\mathbf{m}_2^{\text{mig\_ref}}]=[\mathbf{m}_1^{\text{ref}}]\\ \mathbf{f}_{2,1}*[\mathbf{m}_1^{\text{mig\_ref}}]+\mathbf{f}_{2,2}*[\mathbf{m}_2^{\text{mig\_ref}}]=[\mathbf{m}_2^{\text{ref}}]\end{cases}, \tag{7}$$

where $\mathbf{m}^{\text{ref}}=\begin{pmatrix}\mathbf{m}_1^{\text{ref}}\\ \mathbf{m}_2^{\text{ref}}\end{pmatrix}$ is the reference model and $\mathbf{m}^{\text{mig\_ref}}=\begin{pmatrix}\mathbf{m}_1^{\text{mig\_ref}}\\ \mathbf{m}_2^{\text{mig\_ref}}\end{pmatrix}$ is its corresponding migration image.

We design the $\mathbf{m}^{\text{ref}}$ to be a model with an even distribution of isolated point diffractors in one parameter class, while there are no diffractors in the other parameter class, as shown in Figures 1a and 1c. The reference models are then divided into several subsections centered at the location of each point diffractor. For example, a subsection is displayed as the area of the black squares in Figure 1. In each subsection, $\mathbf{f}_{l,k}$ is assumed to be stationary.

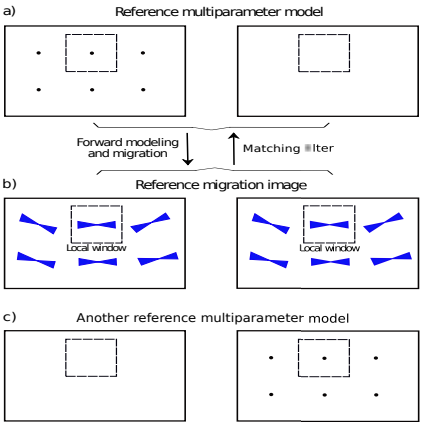

Figure 1: Illustration of local matching filters that transform (b) the migration image $\mathbf{m}^{\text{mig\_ref}}$ to (a) its reference model $\mathbf{m}^{\text{ref}}$. The six black squares belong to the same subsection. Both reference models (a) and (c) are used as input for solving for the filters in equation 7.

NUMERICAL RESULTS

We now test the effectiveness of decoupled deblurring filter on elastic migration and inversion with synthetic elastic data and a marine dataset recorded in the Gulf of Mexico. The synthetic data are simulated from two land models: (1) a layered model with different P- and S-wave velocity anomalies and (2) a portion of the modified Marmousi2 model.

In the synthetic examples, the observed two-component data are generated by a time-space staggered-grid solution of the elastic wave equation (Levander, 1988) without a free-surface boundary condition. The data are used to invert for the P- and S-reflectivity models defined as $\mathbf{m} = (\delta V_p/V_p, \delta V_s/V_s)^T$ using elastic reverse time migration (RTM) and least-squares reverse time migration (LSRTM) (Feng and Schuster, 2016), where V_p and V_s are the background P- and S-wave velocity models and δV_p and δV_s are the corresponding perturbations. Here, the P- and S-reflectivity images are denoted as the P-image and the S-image, respectively. Elastic RTM refers to the first iteration of elastic LSRTM. If a decoupled deblurring filter is not employed, source-side illumination preconditioning (Plessix and Mulder, 2004) is used for both elastic RTM and LSRTM.

Layered velocity model

We first demonstrate that the decoupled deblurring filter can improve the quality of the elastic migration image using the flat-layered elastic model embedded with anomalies in Figure 2. The density is homogeneous with 1 g/cm^3. Here 92 shots are evenly spaced at 50 m, and 230 receivers are evenly distributed at 20 m intervals on the surface. The P-wave point source uses a Ricker wavelet with a 7.5 Hz peak frequency and the total recording time is 5 s.

Figure 3 compares the elastic RTM images with and without the decoupled deblurring filter. The images with filtering have fewer artifacts, better amplitude balancing and higher resolutions compared to the images without filtering. In addition, the P- and S-images without filtering contain false reflectivity images of P- and S-wave velocity anomalies, which are mitigated after applying the filter.

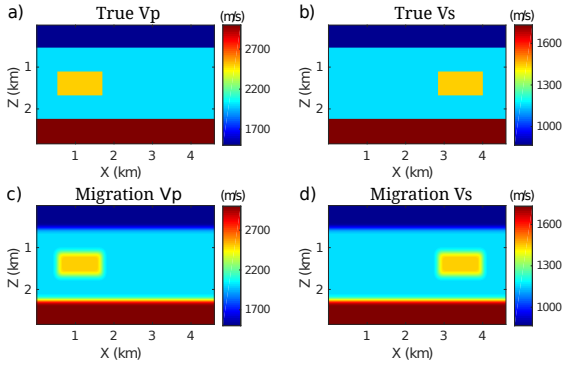

Figure 2: Test models: (a) true V_p, (b) migration V_p, (c) true V_s, and (d) migration V_s.

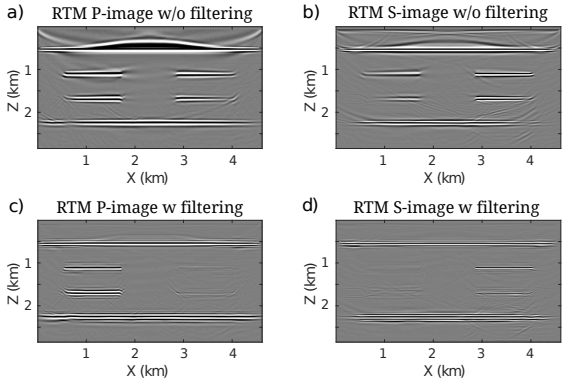

Figure 3: Elastic RTM images of the test model: without filtering for the (a) P-image and (b) S-image, with filtering for the (c) P-image and (d) S-image.

Marmousi2 velocity model

We also demonstrate that the decoupled deblurring filter can be used as a preconditioner to improve the image quality and speed up the convergence rate for elastic LSRTM. Elastic data are generated for a portion of the elastic Marmousi2 model and where the water layer is replaced a solid layer. The S-wave velocity is also modified to avoid very low V_s values. Figures 4a and 4c show the true P- and S-wave velocity models, respectively, and the velocity models for migration are shown in Figures 4b and 4d. The density is constant with 1 g/cm^3. The true reflectivity models for the P- and S-wave velocities are shown in Figure 5. 393 shots are evenly spaced at 20 m, and 787 receivers are evenly distributed at 10 m intervals on the surface. The P-wave point source uses a Ricker wavelet with a 15-Hz peak frequency and the total recording time is 5.5 s.

The elastic RTM images with and without the decoupled deblurring filter are shown in Figure 6. The elastic LSRTM im-

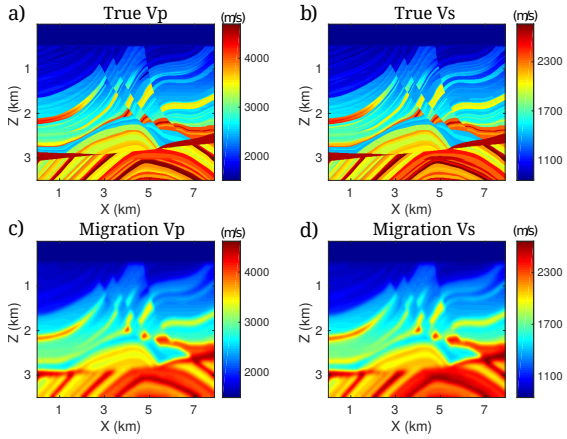

Figure 4: A portion of the modified Marmousi2 model: (a) true V_p, (b) migration V_p, (c) true V_s, and (d) migration V_s.

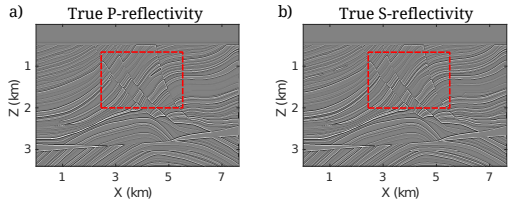

Figure 5: The Marmousi2 reflectivity models: true reflectivity models for the (a) P-wave velocity and (b) S-wave velocity distributions.

ages with and without the filter as a preconditioner are shown in Figure 7. The deblurring filter improves the quality of both the RTM and LSRTM images. It also increases the convergence rate so that the misfit function of LSRTM with the filter at the 6th iteration has about the same value as the one without the filter at the 15th iteration, as shown in Figure 8.

The zoom views of the red-box area (see Figure 5) for the P- and S-images are displayed in Figures 9 and 10, respectively. These magnified views show that the decoupled deblurring filter improves the amplitude balance and resolution of the images. The increase in spatial resolution is further validated by the vertical-wavenumber spectra in Figures 9b and 10b. In the yellow box of Figure 9f, the two reflectors are only distinguishable in the filtered LSRTM P-image. In addition, the RTM S-image without filtering (Figure 10c) shows a strong false structure in the reservoir area, for example, the green box marked in Figures 9a and 10a. These crosstalk artifacts are much weaker in either the LSRTM S-image without filtering (Figure 10d) or the RTM S-image with filtering (Figure 10e). This crosstalk problem is slightly mitigated by LSRTM with filtering, as shown in Figure 10f.

Field data test

The third example is for a 2D marine data set recorded in the Gulf of Mexico. The streamer data consist of 496 shots with a shot interval of 37.5 m. Each shot has 480 hydrophones with

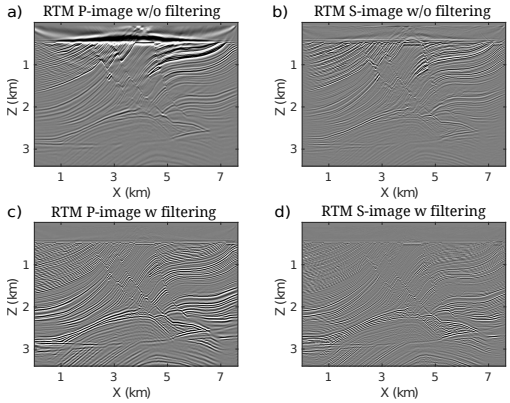

Figure 6: Elastic RTM images of the Marmousi2 model: without filtering for the (a) P-image and (b) S-image, with filtering for the (c) P-image and (d) S-image.

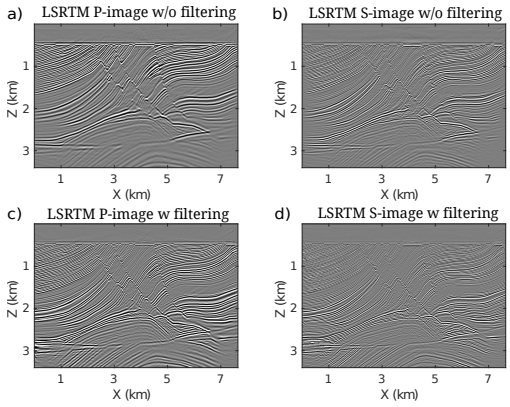

Figure 7: Elastic LSRTM images of the Marmousi2 model: without filtering for the (a) P-image and (b) S-image, with filtering for the (c) P-image and (d) S-image.

a receiver interval of 12.5 m. The maximum source-receiver offset is approximately 6 km, the nearest offset is 198 m, and the recording time is 5 seconds.

Figure 11 compares the elastic RTM images with and without the decoupled deblurring filter. The images with filtering have better amplitude balancing especially for the deeper structures. The images of the shallow reflectors are more continuous and clear because of the better amplitude balancing and higher resolutions.

The residual drops less than 1% for RTM images (first iteration of LSRTM) without filtering while more than 10% with filtering. There is no doubt that there are false reflectivities in the S-image since the marine data set does not contain strong PS converted wave. Here, we mainly demonstrate that decoupled debluring filter can improve the image quality and speed up the convergence rate because it truly approximates the multiparameter Hessian inverse.

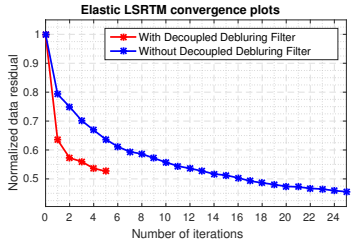

Figure 8: Convergence curves for elastic LSRTM with and without filtering for the Marmousi2 model.

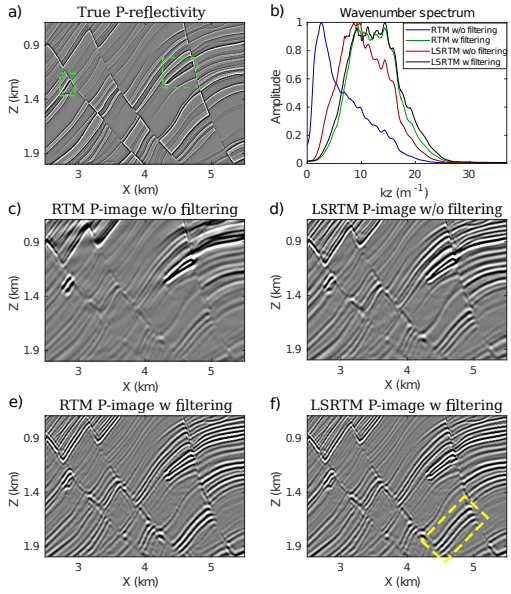

Figure 9: Zoom views showing the P-images in the red boxes in Figures 6 and 7. (a) True P-reflectivity image, (b) vertical-wavenumber spectra, (c) RTM and (d) LSRTM P-images without filtering, (e) RTM and (f) LSRTM P-images with filtering.

CONCLUSION

We estimate the mutiparameter Hessian inverse using local filters to approximate its submatrices for the same and different parameter classes. Numerical tests on the elastic migration and inversion show that the decoupled debluring filter improves the quality of multiparameter migration images and significantly accelerates the convergence speed.

ACKNOWLEDGEMENTS

The research is supported by the King Abdullah University of Science and Technology (KAUST) in Thuwal, Saudi Arabia. We are grateful to the sponsors of the Center for Subsurface Imaging and Modeling (CSIM) Consortium for their financial support. The computation resource provided by the KAUST Supercomputing Laboratory (KSL) is greatly appreciated.

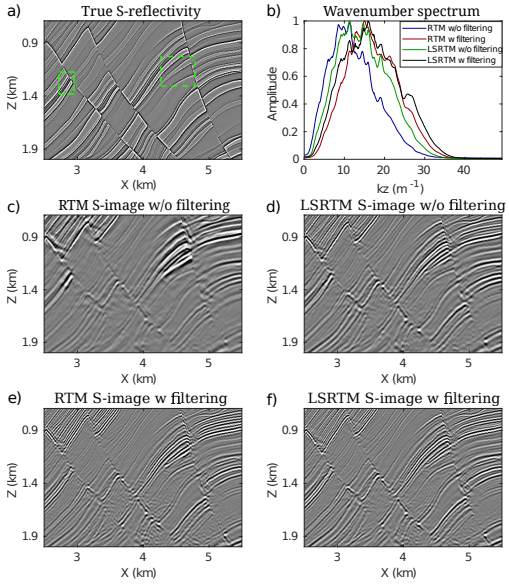

Figure 10: Zoom views showing the S-images in the red boxes in Figures 6 and 7. The figures have the same arrangement as the images in Figure 9.

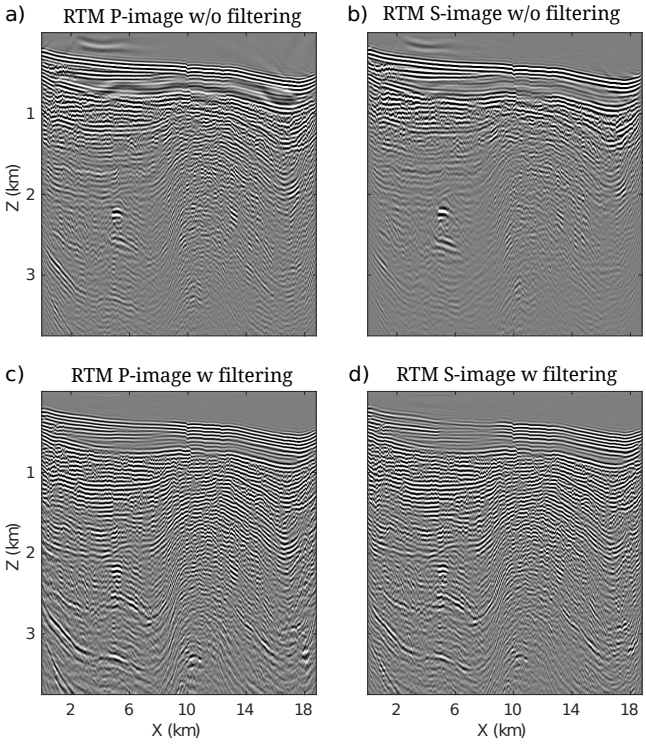

Figure 11: Elastic RTM images of field data test: without filtering for the (a) P-image and (b) S-image, with filtering for the (c) P-image and (d) S-image.